CLEAN Algorithms for Intra-vehicular Time-domain UWB Channel Sounding

Aniruddha Chandra[1], Jiri Blumenstein[1], Tomas Mikulasek[1], Josef Vychodil[1], Martin Pospisil[1], Roman Marsalek[1], Ales Prokes[1], Thomas Zemen[2] and Christoph Mecklenbrauker[3]

[1]*Department of Radio Electronics, Brno University of Technology, Brno, Czech Republic*

[2]*FTW Forschungszentrum, Telekomunikation Wien, Vienna, Austria*

[3]*Institute of Telecommunications, Vienna University of Technology, Vienna, Austria*

Keywords: Deconvolution, CLEAN, Ultra Wide Band, IEEE 802.15.3, Intra-vehicle Communication, Channel Sounding.

Abstract: A comparison of two variants of CLEAN, a time-domain serial subtractive deconvolution algorithm, is presented. Appropriate statistical metrics for assessing the relative merit of the deconvolution technique are identified in the context of intra vehicle ultra wide band transmission, and the better variant was selected based on its performance over a standard IEEE channel simulation testbed. The chosen method is then applied to extract important channel characteristics for a real-world channel sounding experiment performed inside a passenger car.

1 INTRODUCTION

Ultra wide band (UWB) communication is expected to play a key role in the next generation broadband intra vehicle wireless applications (Demir et al., 2014), (Li et al., 2013). The car compartment differs significantly from other well studied indoor/ outdoor environments, and channel sounding experiments are crucial for gaining a thorough knowledge of the UWB signal propagation characteristics in such a medium. A desired feature of any wideband time domain sounding is *super-resolution* capability, i.e. having the potential to distinguish between multi-path components that are separated by a time duration lesser than the channel sounding pulse width. The goal can be attained by time-domain subtractive deconvolution algorithms, popularly known as CLEAN.

Multi-template case specific CLEAN algorithms for UWB were reported in (Yang and Zhang, 2006) and (Muqaibel et al., 2002). However, intra-vehicular measurement literature is not particularly rich in this regard as most of the channel sounding were performed in frequency domain (Demir et al., 2014), (Bas and Ergen, 2013), (Bellens et al., 2011). Time domain experimental papers often lacked detailed discussion on the implementation of algorithm. The only exception is (Niu et al., 2009), where a sub-optimal version of CLEAN is presented. In this paper we show that the modified version of the algorithm can perform much better in intra-vehicular environments. Specifically, our contributions are:

- Presenting discrete versions of CLEAN algorithms that are readily executable through software packages.
- Identifying appropriate statistical metrics for comparing deconvolution methods and validating our choice through standard UWB testbed simulation.
- Deriving channel parameters through deconvolution operation for an in-vehicle channel measurement.

The structure of this paper is as follows. Section 2 provides two working versions of the CLEAN and explains the intricacies of comparison between them. The experimental setup and post-processing of the measured data is presented in Section 3. Finally, Section 4 concludes the paper.

2 DECONVOLUTION

2.1 Ill-posedness

For a causal time-limited input-output waveform set, $\{x(t), y(t)\}$, where $y(t) = x(t) * h(t) + n(t)$, with $*$ denoting the convolution operator and $n(t)$ being the ambient noise, deconvolution of the channel impulse response (CIR), $h(t)$, is, in general, an ill-posed problem. The ill-posedness in deconvolution problem has

Algorithm 1: Basic CLEAN.

STEP 01: **compute** cross-corrlation: $\mathcal{R}^{xy} = x[n] \tilde{*} y[n]$
STEP 02: **initialize** dirty map: $d_0 \leftarrow y$, clean map: $c_0 \leftarrow 0$, threshold: $\mathcal{T} \leftarrow \max|\mathcal{R}^{xy}|/10$, loop gain: $\gamma \leftarrow 0.02$, stopping criterion: $\mathcal{R}_0^* \leftarrow \mathcal{T} + \varepsilon$, $N \leftarrow \text{length}\{y\}$
STEP 03: **while** $|\mathcal{R}_k^*| > \mathcal{T}$ **do**
compute cross-corrlation: $\mathcal{R}_k^{xd} = x[n] \tilde{*} d_k[n]$
find $n_k^* = \arg\max_n |\mathcal{R}_k^{xd}[n]|$, $\mathcal{R}_k^* \leftarrow \mathcal{R}_k^{xd}[n_k^*]$
shift input $x^s[n] = x[n - n_k^s]$; $n_k^s = N - n_k^*$
clean dirty map: $d_k \leftarrow d_{k-1} - \gamma \mathcal{R}_k^* x^s$
if $(0 < n_k^s < N)$
update clean map: $c_k[n_k^s] \leftarrow c_{k-1}[n_k^s] + \gamma \mathcal{R}_k^*$
end if
end while
STEP 04: **return** $\hat{h} \leftarrow c$

has two aspects, first, there is no *unique* solution, and second, the solution procedure is often *unstable*. The instability is reflected in the attempt of a direct frequency-domain inversion $H(\omega) = Y(\omega)/X(\omega)$ which leads to erroneous computation of $h(t)$ as the noise component in $Y(\omega)$ may not be small when $X(\omega) \simeq 0$.

The lack of a direct inverse operation gave rise to multiple deconvolution methods. However, only few of them are having super-resolution capability. The non-iterative algorithms are mostly maximum likelihood estimator based (EM, SAGE etc.), and they suffer heavily from the noise induced instability problems. This makes the iterative CLEAN algorithms a natural choice.

2.2 Variants of CLEAN

In this paper, we present the basic CLEAN (Vaughan and Scott, 1999) and a modified CLEAN (Liu et al., 2007) algorithm. The basic algorithm assumes a linear time-invariant tapped delay line model for the channel, and through successive iterations, extracts the CIR (clean map) by subtracting shifted input signal replicas from the output (dirty map). For the modified algorithm, subtraction takes place in the convolution domain. Both the algorithms are readily implementable in popular software packages (e.g. MATLAB) as they work on the discrete version of the time-domain input-output waveforms, $x[n]; n \in \mathbb{Z}^*_{\leq N_1}$ and $y[n]; n \in \mathbb{Z}^*_{\leq N_2}$. Before feeding the sequences, appropriate zero-padding is required to make the length of the sequences equal to N, where $N = \max\{N_1, N_2\}$. Further, the discrete cross-correlation operator, $\tilde{*}$, is defined as $\mathcal{R}^{xy}[n] = x[n] \tilde{*} y[n] = \hat{R}^{xy}[n - N]$, where $\hat{R}^{xy}[n] = \sum_{k=0}^{N-n-1} x[n+k]y[k]$ for $n \geq 0$ and $\hat{R}^{xy}[n] = \hat{R}^{yx}[-n]$ for $n < 0$.

The stopping criterion may be chosen to attain a target energy capture ratio, $ECR = [1 - \{||y - \hat{y}||/||y||\}^2] \times 100\%$, where $\hat{y}(t) = x(t) * \hat{h}(t)$ denotes the reconstructed output generated using the estimated response $\hat{h}(t)$, or to maintain a dynamic range, $DR = 20\log_{10}[\max(\hat{h})/\min(\hat{h})]$. In this paper, we considered a threshold, $\mathcal{T}$, equal to 10% of the peak cross-correlation value. A higher value caused missing of significant multi-path components (MPCs), while a lower threshold generated too many paths by picking up noise.

In order to demonstrate the leverages of the modified algorithm, we would like to point out: (i) the presence of loop gain in the basic algorithm, the choice of which is often empirical and case-dependent, (ii) avoiding the necessity of calculating correlation at each iteration, and (iii) an absolute assignment of a MPC during updation of clean map, which was not possible for the basic case because the residues of the signal in some earlier iteration may result in an update.

2.3 Comparison

The sinusoidally modulated Gaussian pulse used for intra vehicular UWB channel sounding (Section 3) has the form

$$x(t) = \sqrt{\frac{2\sqrt{2}}{t_d\sqrt{\pi}}} \exp\left[-\left(\frac{t}{t_d}\right)^2\right] \cos(2\pi f_c t + \phi) \quad (1)$$

having unit energy, initial phase $\phi = 0.6\pi$, and an effective pulse duration of $2t_d = 0.276$ns on either side. The carrier frequency, $f_c = 6.5$GHz, was set at the middle of the FCC approved band (3GHz to 10GHz). From Figure 1, it is easy to understand the rationale behind choosing a Gaussian sine pulse over the popular Gaussian doublet: a flatter spectrum (-20 dB bandwidth is almost 1.5 times), reduced low-frequency components which aids antenna radiation, and a better compliance with the outdoor and vehicular radar UWB emission masks. The arguments hold true for

Algorithm 2: Modified CLEAN.

STEP 01: **compute** cross-corrlation: $\mathcal{R}^{xy} = x[n] \tilde{*} y[n]$
STEP 02: **compute** auto-corrlation: $\mathcal{R}^{xx} = x[n] \tilde{*} x[n]$
STEP 03: **initialize** dirty map: $d_0 \leftarrow \mathcal{R}^{xy}$, clean map: $c_0 \leftarrow 0$, threshold: $\mathcal{T} \leftarrow \max|\mathcal{R}^{xy}|/10$, stopping criterion: $d_0^* \leftarrow \mathcal{T} + \varepsilon$, $N \leftarrow$ length $\{y\}$
STEP 04: **while** $|d_k^*| > \mathcal{T}$ **do**
  find $n_k^* = \arg\max_n |d_k[n]|$, $d_k^* \leftarrow d_k[n_k^*]$
  shift auto-correlation $\mathcal{R}^{xx,s}[n] = \mathcal{R}^{xx}[n + n_k^s]$; $n_k^s = N - n_k^*$
  clean dirty map: $d_k \leftarrow d_{k-1} - d_k^* \mathcal{R}^{xx,s}$
  if $(0 < n_k^s)$
    update clean map: $c_k[n_k^s] \leftarrow d_k^*$
  end if
end while
STEP 05: **return** $\hat{h} \leftarrow c$

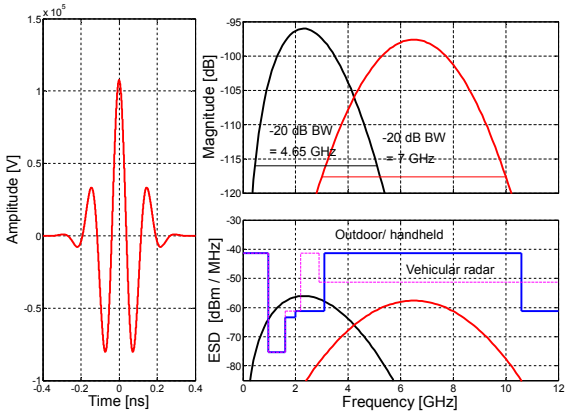

Figure 1: Input pulse $x(t)$ [left], it's amplitude spectra $X(f)$ [right-top], and compliance with FCC UWB emission masks [right-bottom]. The black curves depict the frequency-domain characteristics for the Gaussian 2nd derivative with equivalent parameters (unit energy and same t_d).

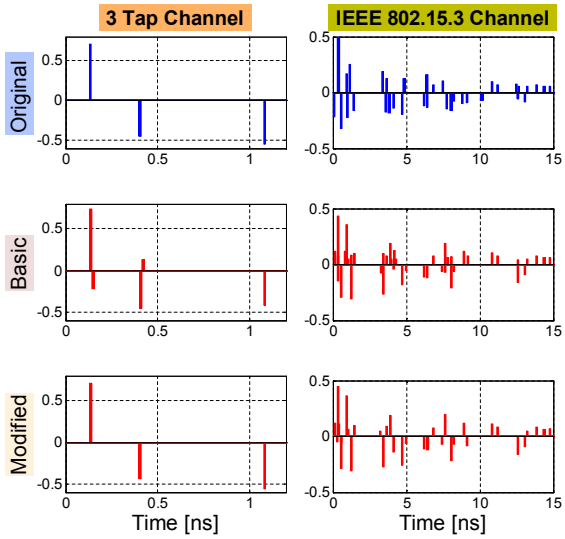

Figure 2: Comparison of the estimated CIRs with the original CIR (SNR = 10dB, $\gamma = 0.02$).

other baseband pulses too (e.g. raised cosine pulse that obey Nyquist criterion).

For comparison, we have convolved the input signal given in (1) with some energy normalized $(\sum_n h^2[n] = 1)$ synthetic impulse response, added Gaussian noise, and applied the algorithms described in Section 2.2 to estimate the CIRs. Although, the common strategy is to match the reconstructed signal $\hat{y}(t)$ against the original received signal $y(t)$, we compared $\hat{h}(t)$ directly with $h(t)$ to see which method provides better representation of the multipath nature of the channel.

The test is first performed for a simple 3 tap channel with tap gains separated by a distance less than the pulse width. A casual inspection of the reconstruction results (Figure 2 [left]) reveals that the modified method results less spurious components, and the ratio between CIR taps are better maintained.

Next we simulated the discrete version of the standard UWB IEEE 802.15.3 channel based on modified Saleh-Valenzuela model (Molisch et al., 2003). The simulation parameters for CM1/CM2 (0-4 m) were assumed to resemble the intra-vehicular environment, and only significant paths within 10dB of the peak have been retained. Comparison of the estimated CIR profiles (Figure 2 [right]) is no longer possible through visual inspection. In fact, assessing relative merits of two solutions for an ill-posed problem is subjective to the metric used. For example, measuring the number of significant MPCs is not very meaningful, the multipath profile depends not only on number of taps, but also on their respective delays. Another crude method is to compare the mean square error (MSE), $\sum_{n=1}^{N}(\hat{h}[n] - h[n])^2/N$. However, the results averaged over 1000 channel samples indicated marginal improvement (3-4%) of the MSE.

A better conclusion may be reached by resorting to statistical comparisons. The parameter we use here is Kullback-Leibler (KL) divergence

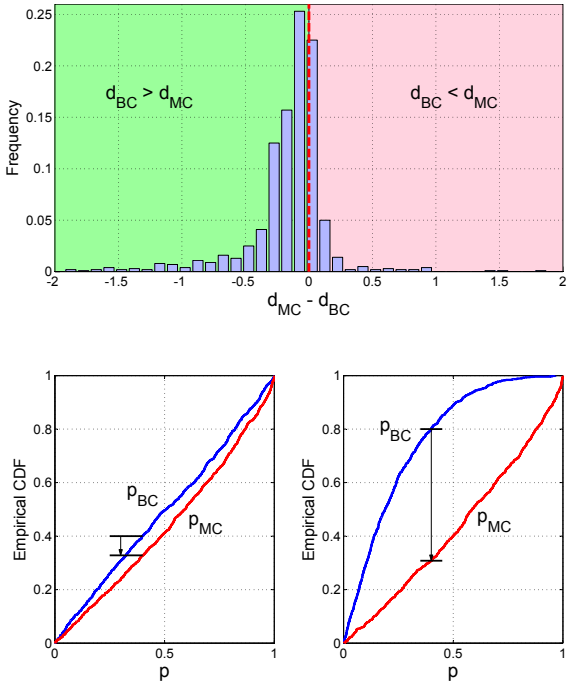

Figure 3: [Top] Histogram of difference of KL distance. [Bottom] Comparison of CDF of p-values for $\gamma = 0.02$ and $\gamma = 0.03$.

$$d = \sum_{n=1}^{N} h[n] \log_2 \left(\frac{h[n]}{\hat{h}[n]} \right) \quad (2)$$

which measures the distance between common non-zero elements of the CIR vector. Note that the suffixes (BC and MC) are used to signify the basic CLEAN and modified CLEAN algorithms.

A negative skewness of the histogram (Figure 3 [top]) of the difference of the distances vouch for the superiority of the modified algorithm. The plot portrays, how often, on an average, the CIRs constructed with the modified algorithm differ less than that obtained through the basic algorithm.

Next, we performed a two-sample Kolmogorov-Smirnov test. The test is different from the earlier test in the sense that it does not judge the one-to-one correlation, rather it focuses on the similarity of the inherent random distribution of CIR tap gains. The Kaplan-Meier estimate of the cumulative distribution function (CDF) of the p-values, measured against a 5% significance level, are shown in Figure 3 [bottom]. The CDF for the basic algorithm exceeds the modified one, implying that the probability of obtaining smaller p-values for the basic case is more. The sensitivity of the basic algorithm to parameter setting is also quite self explanatory. When the loop gain (γ) changes slightly from 0.02 to 0.03, the gap between the CDFs widens drastically.

3 MEASUREMENT SETUP AND RESULTS

The UWB time domain channel sounding measurements were performed in a mid-sized passenger car Skoda Octavia III under static (not moving) condition. The Gaussian sine pulse generated through the Tektronix AWG70002A waveform generator was first amplified through a high power amplifier (HPA) before feeding the signal to a wideband conical monopole antenna. At the receiver side an identical antenna is placed which receives the signal. The signal is then amplified through a low noise amplifier (LNA) and viewed/ stored in a digital sampling oscilloscope Tektronix DPO72004C. Figure 4 depicts the interconnections of the apparatus and close-ups of antenna positioning.

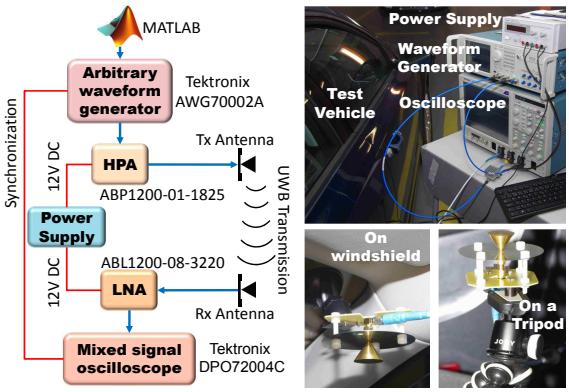

Figure 4: [Clockwise from left] Block diagram of the measurement setup, picture of the apparatus, and antenna close-ups (tripod and right windscreen).

As shown in Figure 5, a total of 52 different Tx-Rx antenna positions, with separations ranging from 0.56m to 1.9m, were tested with different degrees of passenger occupancy. Some measurements were repeated to investigate temporal variation, which were found to be negligible.

The received signal, $y(t)$, for a particular measurement can be represented as

$$y(t) = x(t) * h_{Tx,Ant} * h(t) * h_{Rx,Ant} = x_{ref}(t) * h(t) \quad (3)$$

where $h_{Tx,Ant}$ and $h_{Rx,Ant}$ are the impulse responses of the transmitter (Tx) and receiver (Rx) antennas, and $x_{ref}(t) = x(t) * h_{Tx,Ant} * h_{Rx,Ant}$ is the reference input *template* that was obtained by measuring the response of the input $x(t)$ in an anechoic chamber free from reflectors/ diffractions. Next, multipath intensity profiles were obtained by deconvolving the received signals with the input template using the modified CLEAN algorithm. Samples of the post processing of data is shown in Figure 6 for two indicative

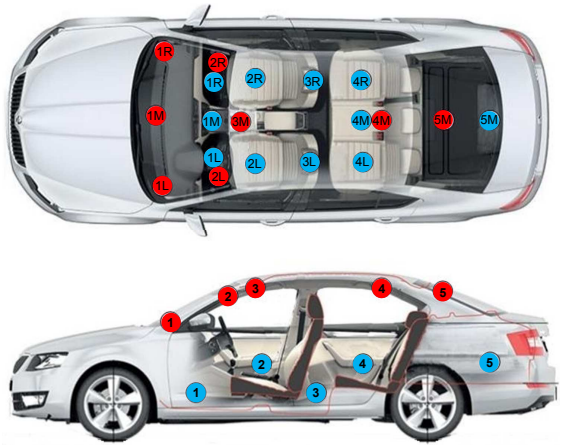

Figure 5: Antenna placement in the car, RED: Tx antennas, BLUE: Rx antennas.

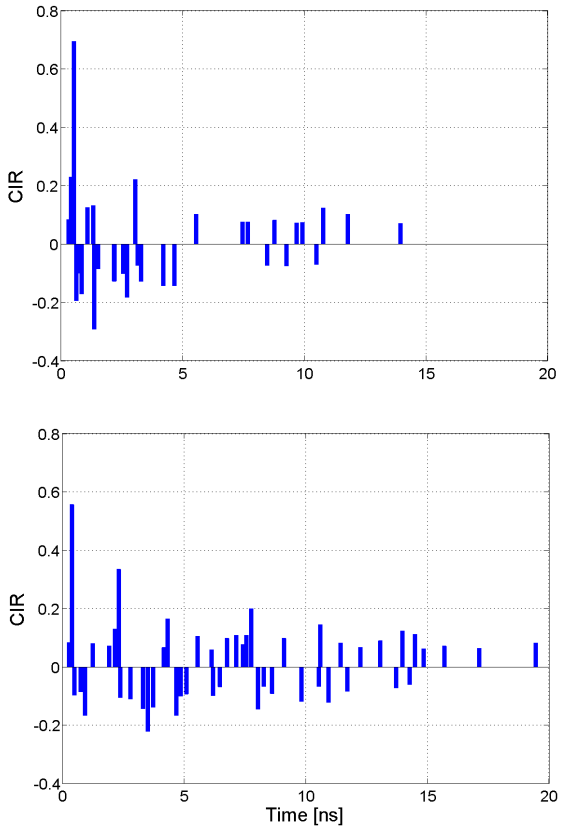

Figure 6: Extracted CIR for LoS (Tx: 2L, Rx: 2R) condition [Top] and nLoS (Tx: 2L, Rx: 4R) condition [Bottom].

cases with no passengers and the Tx antenna set at the left side of the windscreen near the roof (2L in Figure 5); first when Rx antenna is placed on a tripod on the driver seat (2R in Figure 5) creating a direct line-of-sight (LoS) propagation path and next for a non-LOS (nLoS) transmission with the Rx antenna on the rear passenger seat on right (4R in Figure 5) with similar tripod arrangements. The number of MPC is quite higher for the nLoS case as expected.

Table 1: Variation of RMS delay spread with passenger occupancy. Tx and Rx antenna positions are as per markings in Figure 5. Passenger legends are, D: driver, FP: front passenger, RL: rear passenger on left.

Rx pos.	Tx pos.	Tx-Rx gap [cm]	Passenger	τ_{rms} [ns]
4R	1L	182	–	6.8880
”	”	”	D	6.3442
”	”	”	D, FP	5.6712
”	”	”	D, FP, RL	4.9847
”	2L	146	–	5.8361
”	”	”	D	5.1931
”	”	”	D, FP	4.6487
”	1R	162	–	9.4691
”	”	”	D	8.4802
”	”	”	D, FP	7.8969
”	2R	119	–	7.9445
”	”	”	D	7.9668
”	”	”	D, FP	7.4689
”	5M	83	–	3.4871
”	”	”	D	2.7340
”	”	”	D, FP	2.9521
2R	4M	123	–	6.1866
”	”	”	FP	5.6423
”	”	”	FP, RL	3.9350
”	5M	161	–	7.0158
”	”	”	FP	6.1101
”	”	”	FP, RL	5.1240
”	2L	97	–	2.6203
”	”	”	FP	2.0125
”	”	”	FP, RL	2.1586
”	1L	118	–	4.7816
”	”	”	FP	3.9739
”	”	”	FP, RL	3.4004

The CIR profiles obtained after the post-processing via CLEAN can be utilized to extract various channel parameters such as number of MPCs, mean excess delay, etc. Nevertheless, our discussions here are limited to root mean square (RMS) delay spread which is not much susceptible to apparatus settings and synchronization. RMS delay spread is defined as the second central moment of the average power delay profile, and can be calculated through the formula

$$\tau_{rms} = \sqrt{\frac{\sum_n \tau_n^2 |\hat{h}_n|^2}{\sum_n |\hat{h}_n|^2} - \left[\frac{\sum_n \tau_n |\hat{h}_n|^2}{\sum_n |\hat{h}_n|^2}\right]^2} \qquad (4)$$

where $\{\tau_n, \hat{h}_n\}$ are the delay and gain associated with the nth path.

Interestingly, when RMS delay spread values were examined for different Tx-Rx distances, only a weak correlation was observed. On the other hand, as seen from Table 1, τ_{rms} decreased consistently with higher passenger occupancy across all different Tx-Rx settings. The reduction in delay spread can be accounted for the obstruction and absorption of several MPCs by human body.

4 CONCLUSIONS

In this paper, we investigated two versions of CLEAN algorithm for estimating CIR in intra-vehicular UWB channel sounding experiment. The efficacy of the modified CLEAN algorithm over the basic version is established through statistical measures. Next, using the modified algorithm, post-processing of time domain channel measurement data were performed. The results show that while the RMS delay spread is weakly dependent on the antenna separation, it decreases linearly with passenger occupancy.

We believe that CLEAN algorithms presented in the current text would simplify human-computer interactions for the wireless physical layer experimentalists, and would be appealing to those who are working towards realization of intelligent transportation systems. Our project team is currently developing a more sophisticated spread spectrum based channel sounding system, and we would like to study the suitability of these algorithms for the new setup.

ACKNOWLEDGEMENTS

This work was supported by the SoMoPro II programme, Project No. 3SGA5720 *Localization via UWB*, co-financed by the People Programme (Marie Curie action) of the Seventh Framework Programme of EU according to the REA Grant Agreement No. 291782 and by the South-Moravian Region. The research is further co-financed by the Czech Science Foundation, Project No. 13-38735S *Research into wireless channels for intra-vehicle communication and positioning*, and was performed in laboratories supported by the SIX project, No. CZ.1.05/2.1.00/03.0072, the operational program *Research and Development for Innovation*. The generous support from Tektronix, Testovací Technika, and Skoda a.s. Mlada Boleslav are also gratefully acknowledged.

REFERENCES

Bas, C. U. and Ergen, S. C. (2013). Ultra-wideband channel model for intra-vehicular wireless sensor networks beneath the chassis: from statistical model to simulations. *IEEE Trans. Veh. Tech.*, 62(1):14–25.

Bellens, F., Quitin, F., Dricot, J. M., Horlin, F., Benlarbi-Delaï, A., and Doncker, P. D. (2011). A wideband channel model for intravehicular nomadic systems. *Int. J. Ant. Prop.*, 2011(468072):1–9.

Demir, U., Bas, C. U., and Ergen, S. C. (2014). Engine compartment UWB channel model for intravehicular wireless sensor networks. *IEEE Trans. Veh. Tech.*, 63(6):2497–2505.

Li, B., Zhao, C., Zhang, H., Sun, X., and Zhou, Z. (2013). Characterization on clustered propagations of UWB sensors in vehicle cabin: measurement, modeling and evaluation. *IEEE Sensors J.*, 13(4):1288–1300.

Liu, T. C. K., Kim, D. I., and Vaughan, R. G. (2007). A high-resolution, multi-template deconvolution algorithm for time-domain UWB channel characterization. *Can. J. Elect. Comput. Eng.*, 32(4):207–13.

Molisch, A. F., Jeffrey, R. F., and Marcus, P. (2003). Channel models for ultrawideband personal area networks. *IEEE Wireless Commun.*, 10(6):14–21.

Muqaibel, A., Safaai-Jazi, A., Woerner, B., and Riad, S. (2002). UWB channel impulse response characterization using deconvolution techniques. In *Proc. IEEE MWSCAS*, volume 3, pages 605–08, Tulsa, OK, USA.

Niu, W., Li, J., and Talty, T. (2009). Ultra-wideband channel modeling for intravehicle environment. *EURASIP J. Wirel. Commun. Net.*, 2009(806209):1–12.

Vaughan, R. G. and Scott, N. L. (1999). Super-resolution of pulsed multipath channels for delay spread characterization. *IEEE Trans. Commun.*, 47(3):343–47.

Yang, W. and Zhang, N. (2006). A new multi-template CLEAN algorithm for UWB channel impulse response characterization. In *Proc. IEEE ICCT*, pages 1–4, Guilin, China.